2019

Double deletion of Panx1 and Panx3 affects skin and bone but not hearing

J M. Abitbol
Western University

B L. O'Donnell
Western University

C B. Wakefield
Western University

E Jewlal
Western University

J J. Kelly
Western University

See next page for additional authors

Journal of Molecular Medicine (2019) 97:723–736
https://doi.org/10.1007/s00109-019-01779-9

JMolMed

ORIGINAL ARTICLE

Double deletion of *Panx1* and *Panx3* affects skin and bone but not hearing

J. M. Abitbol[1] · B. L. O'Donnell[1] · C. B. Wakefield[1] · E. Jewlal[1] · J. J. Kelly[1] · K. Barr[1] · K. E. Willmore[1] · B. L. Allman[1] · S. Penuela[1]

Received: 3 November 2018 / Revised: 11 March 2019 / Accepted: 13 March 2019 / Published online: 27 March 2019

Abstract

Pannexins (Panxs), large-pore channel forming glycoproteins, are expressed in a wide variety of tissues including the skin, bone, and cochlea. To date, the use of single knock-out mouse models of both Panx1 and Panx3 have demonstrated their roles in skin development, bone formation, and auditory phenotypes. Due to sequence homology between Panx1 and Panx3, when one Panx is ablated from germline, the other may be upregulated in a compensatory mechanism to maintain tissue homeostasis and function. To evaluate the roles of Panx1 and Panx3 in the skin, bone, and cochlea, we created the first Panx1/Panx3 double knock-out mouse model (dKO). These mice had smaller litters and reduced body weight compared to wildtype controls. The dKO dorsal skin had decreased epidermal and dermal area as well as decreased hypodermal area in neonatal but not in older mice. In addition, mouse skull shape and size were altered, and long bone length was decreased in neonatal dKO mice. Finally, auditory tests revealed that dKO mice did not exhibit hearing loss and were even slightly protected against noise-induced hearing damage at mid-frequency regions. Taken together, our findings suggest that Panx1 and Panx3 are important at early stages of development in the skin and bone but may be redundant in the auditory system.

Key messages

- Panx double KO mice had smaller litters and reduced body weight.
- dKO skin had decreased epidermal and dermal area in neonatal mice.
- Skull shape and size changed plus long bone length decreased in neonatal dKO mice.
- dKO had no hearing loss and were slightly protected against noise-induced damage.

Keywords Pannexin · Hearing · Skin · Bone · Panx1 · Panx3

Introduction

Pannexins (Panxs; Panx1, Panx2, and Panx3), are a family of three glycoproteins that form large pore channels at the plasma membrane [1–3] to allow passage of ions and metabolites through the intracellular and extracellular space [4, 5]. Panx1 is expressed in most mammalian organs [2, 6–10], while Panx2 has been found to have a more restricted expression pattern [2, 11]. Panx3 has been reported to be expressed predominantly in the skin, cartilage, and bone [2, 9, 12].

Panx1 plays a role in many cellular processes such as ATP release, Ca^{2+} wave propagation, and apoptosis [13–15]. Panx1 channels can be opened through mechanical stimulation, an increase in intracellular calcium concentration, extracellular potassium concentration, membrane depolarization, as well as caspase 3 cleavage [13–16]. Panx1 is highly expressed in young mouse skin, but decreases in aged skin [17] and is important in keratinocyte differentiation [18]. We previously found that $Panx1^{-/-}$ (KO) mice had reduced dermal area, but increased hypodermal thickness in dorsal skin compared to wild-type (WT) mice [17]. $Panx1^{-/-}$ mice displayed increased

B. L. Allman and S. Penuela are senior authors

Electronic supplementary material The online version of this article (https://doi.org/10.1007/s00109-019-01779-9) contains supplementary material, which is available to authorized users.

✉ S. Penuela
spenuela@uwo.ca

[1] Department of Anatomy and Cell Biology, Schulich School of Medicine and Dentistry, University of Western Ontario, London, ON N6A 5C1, Canada

fibrosis and delayed wound healing [17]. Panx3 is also expressed in adult human skin and embryonic mouse skin tissues and participates in wound healing [16, 18–20].

Panx3 is found in bone and cartilage tissues [21, 22] and is involved in the differentiation of osteoblasts [23]. Panx3 is also expressed in pre-hypertrophic chondrocytes and acts to accelerate their terminal differentiation through increased ATP release [21]. Our group previously generated a global Panx3$^{-/-}$ (KO) mouse that was shown to be less prone to surgically induced osteoarthritis [24]. Although gross skeletal phenotypic changes were not observed in this global Panx3$^{-/-}$ mice, analyses of micro-CT images of long bones of adult Panx3$^{-/-}$ and WT mice revealed that KO mice had shorter long bone diaphyses, larger areas of muscle attachment, and greater cross-sectional areas at mid-diaphysis compared to WT mice [25].

Our group has recently shown that the global Panx1$^{-/-}$ mouse did not exhibit hearing loss nor changes in the timing/amplitude of the sound-evoked electrical activity recorded in the auditory brainstem [26]. In contrast, studies using conditional ablation of Panx1 in the cochlea exhibited severe hearing loss at all frequencies, reduced endocochlear potential, and reduced cochlear microphonics [27, 28]. In a recent study, we investigated the role of Panx1 and Panx3 in noise-induced hearing loss. Although no differences were found between Panx1$^{-/-}$ mice and their WT littermates, Panx3$^{-/-}$ mice had slightly better hearing recovery after noise exposure than WT mice [26].

Illustrating the potential compensation between pannexins, single Panx1$^{-/-}$ and Panx2$^{-/-}$ mice were subjected to ischemic stroke and had similar degrees of infarcts compared to controls [29]. However, Panx1/Panx2 double knock-out mice had smaller infarct sizes to the brain and better central nervous system functional outcomes, suggesting that ablation of both genes was necessary to observe the phenotype [29].

Panx1 and Panx3 share protein sequence homology, and thus, it is postulated that the lack of gross overt phenotypes observed in one Panx null mouse modelcould be due to functional compensation. In fact, Panx3 was upregulated in the skin, blood vessels, and the vomeronasal organ of Panx1$^{-/-}$ mice [17, 30, 31]. To address this compensation issue, we have generated the first Panx1 and Panx3 double knock-out mouse (dKO) and focused our characterization on the skin, bone, and the auditory system that are known to express both pannexins.

Materials and methods

Generation of dKO mice

Panx3$^{-/-}$ mice were generated in house [24]. Panx1$^{-/-}$ mice were a kind gift from Genentech Inc. (San Francisco, CA) and were previously described [32]. Panx3$^{-/-}$ mice were crossed with Panx1$^{-/-}$ mice to generate offspring heterozygous (HT) for both Panx. These mice were backcrossed with either Panx3$^{-/-}$ or Panx1$^{-/-}$ mice to generate Panx1$^{\pm}$/Panx3$^{-/-}$ or Panx1$^{-/-}$/Panx3$^{\pm}$. The HT/KO and KO/HT mice were crossed, and mice null for both pannexins (dKO) were selected and kept in a closed colony. C57BL/6 mice were used as controls. Mice were maintained on a 12-h-light to 12-h-dark cycle and fed ad libitum. All experiments followed the guidelines and protocols for animal care approved by the Animal Care Committee at the University of Western Ontario.

Genotyping

Tail tips from P4–5 were digested in EDTA in a protein kinase solution. PCR was used to verify the lack of exon 2 in both genes. Primers are listed in Suppl. Table 1. Panx1 #1 flank floxed exon 2 and yields a 662-bp WT DNA and a 450-bp Panx1 KO fragment. For Panx3, two reactions were needed. Reaction 1 uses Panx3 #1 primers flanking exon 2 and yield a 1326 bp WT DNA fragment and a 600-bp DNA fragment indicates at least one mutant allele. To distinguish between a Panx3 HT or full KO, a second reaction is conducted using Panx3 #2 primers where WT and Panx3 HT mice produce a 770 bp band, not seen in a Panx3 KO.

Ribonucleic acid extraction and quantitative polymerase chain reaction

Two to 3-month-old cochleae, P4-P5 skin, and P4-P5 hindlimb tissues were dissected from mice and flash-frozen in liquid nitrogen. Ribonucleic acid (RNA) was extracted using a combination of Trizol and a Qiagen RNeasy mini kit as was previously described [26]. Primers used are listed in Suppl. Table 1. Normalized mRNA expression levels were analyzed using the delta delta CT method which was calculated using BioRad CFX Manager Software.

Protein extraction and immunoblotting

Protein was extracted from P4-P5 skin and hind limb tissues. Fifty micrograms of protein were run on a gel and immunoblotted for Panxs. Positive controls of Panx1 or 3 were ectopically expressed in HEK 293T cells (ATCC) as previously described [17] (details in Suppl. Methods).

Histology

Histology assays were performed on skin samples collected from WT and dKO male mice at various ages. Measurements

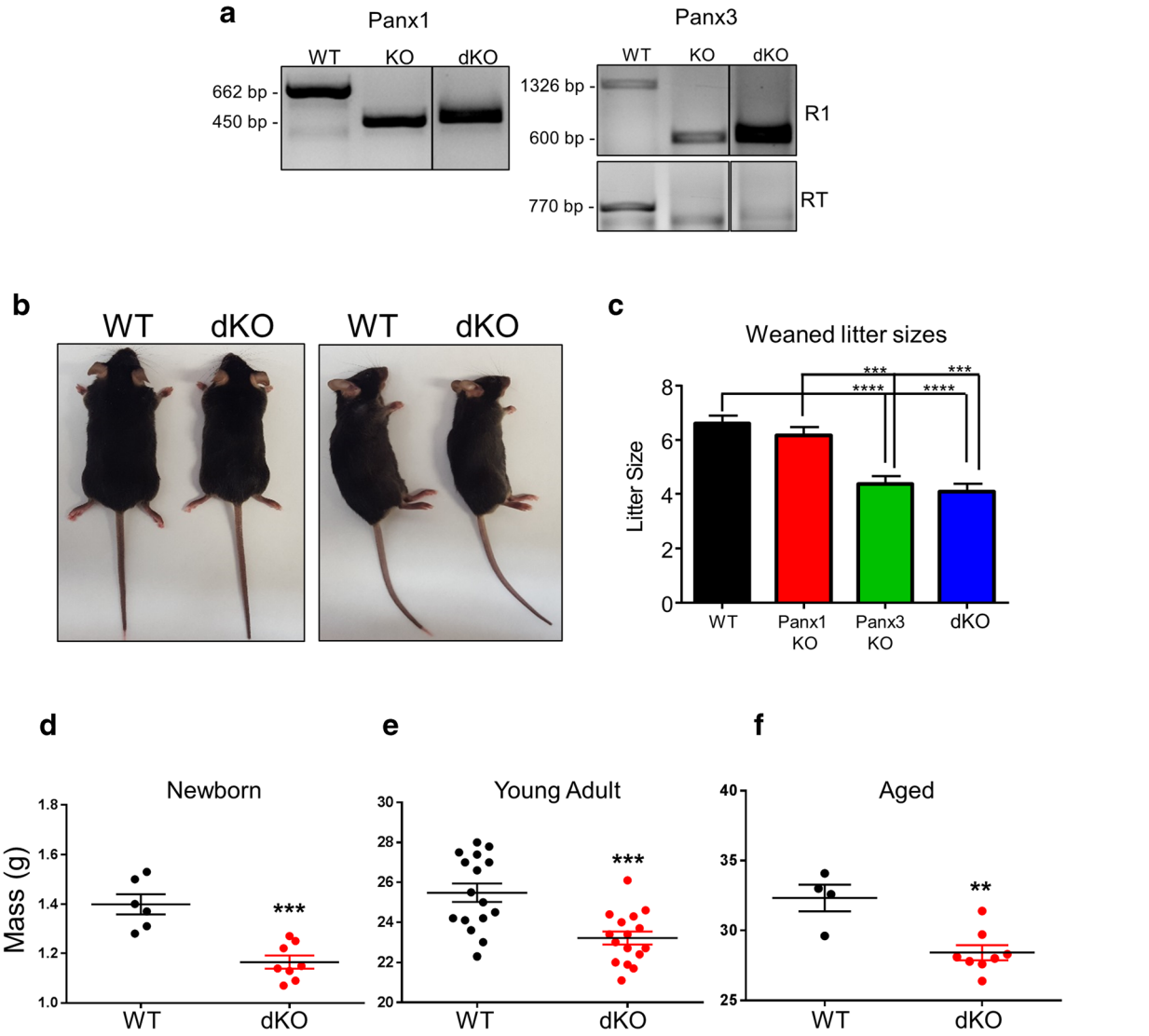

Fig. 1 Characterization of dKO mice. Representative genotyping gels for dKO and WT mice for Panx1 and Panx3 exon 2 deletions. R1, reaction 1 (primers Panx3F1 and reverse Panx3R1) primers flank exon 2 and yield a 1326-bp WT DNA fragment and a 600-bp DNA fragment which shows the presence of at least one mutant allele. To distinguish between Panx3 HT or full KO, a second reaction (RT) is conducted using Panx3F1 and reverse Panx3RT that yields a 770-bp in the WT but not in the KO. Lines denote lanes from the same gel shown after removal of extra lanes (**a**). Representative pictures of WT and Panx1$^{-/-}$Panx3$^{-/-}$ mice at 3 months of age (**b**). Litter sizes of WT, Panx1$^{-/-}$, Panx3$^{-/-}$, and dKO mice at time of weaning where $N = 71$, 49, 45, and 36, respectively, one-way ANOVA followed by post-hoc Tukey's test (**c**). Body weights of postnatal day 0 (P0) (WT: $N = 6$, dKO: $N = 8$), 2–3-month-old (WT: $N = 16$, dKO: $N = 16$), and 16-month-old (WT, $N = 4$ and dKO, $N = 8$) WT and dKO mice (**d**–**f**). Unpaired students t tests $^{**}p < 0.01$, $^{***}p < 0.001$, $^{****}p < 0.0001$. N, number of biological replicates

from dKO and WT samples were compared using unpaired sample t tests (GraphPad Prism 7).

Skull shape and size comparisons-imaging

Micro-computed tomography (μCT) images were obtained from a sample of dKO and WT mice at P0, and at 3 months. Images were obtained at an isotropic voxel size of 20 μm and reconstructed as 3D volumes. Adult mouse skulls were scanned with the eXplore speCZT μCT scanner (GE Healthcare, Waukesha, WI, USA). (details in Suppl. Methods).

Data collection: landmarking

Surface reconstructions were generated from μCT volumes of each skull, and 3D landmark coordinate data was collected using Checkpoint (Stratovan Corporation, Davis, CA, USA). A set of 45 and 53 homologous skull landmarks as well as 19 homologous mandibular landmarks were collected from P0 and 3-month-old mice, respectively [33, 34]. Two landmark trials were conducted by the same observer and deviations between the two trials were restricted to 0.05 mm [35] and then averaged for further analyses.

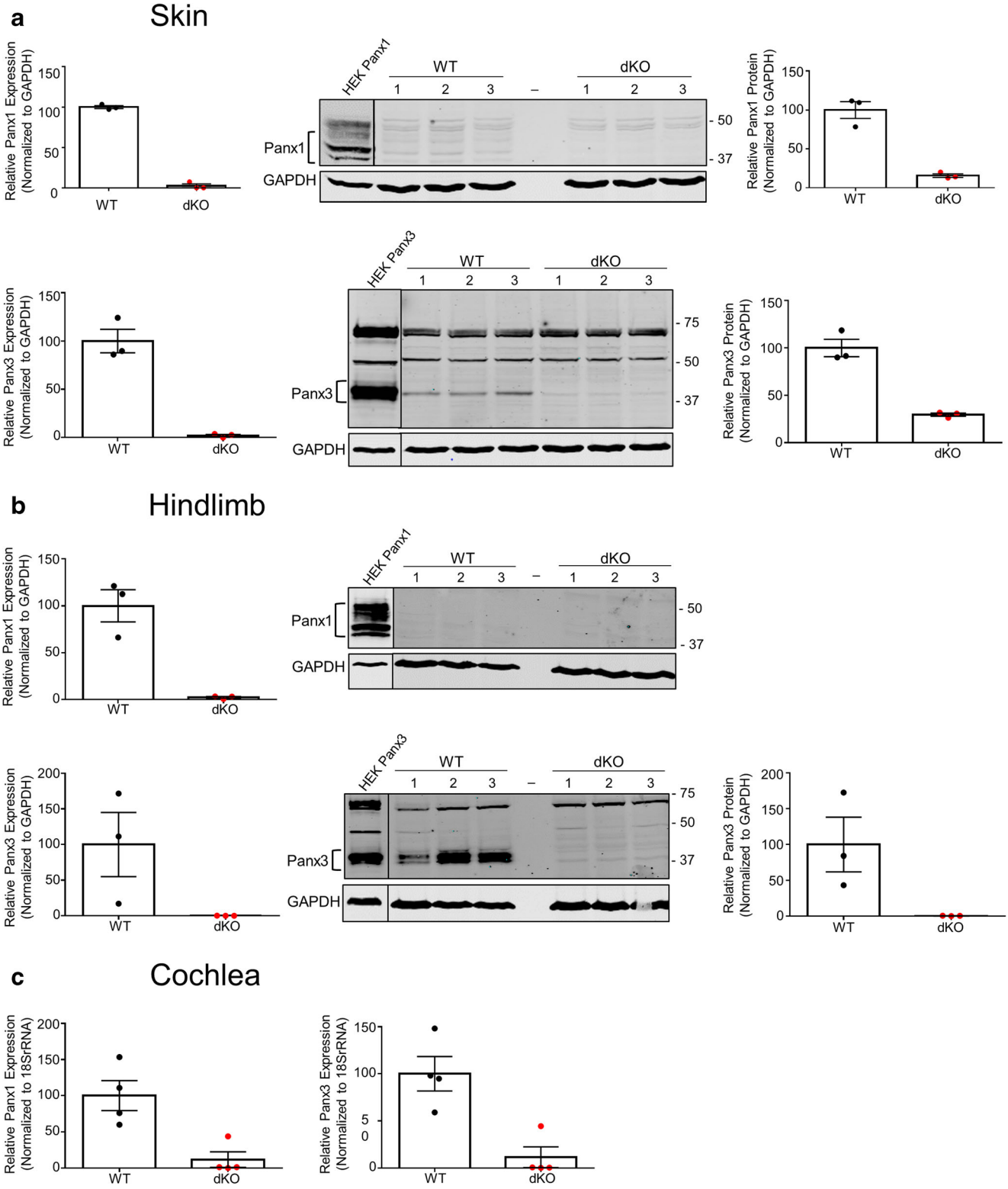

Geometric morphometric analyses—skull shape and size

Geometric morphometric statistical analyses were used for quantification and comparison of subtle shape and size differences. Landmark data underwent Procrustes superimposition using the R package *geomorph* [36, 37] (R Foundation for Statistical Computing, Vienna, Austria, 2017), and subsequent analyses were conducted on Procrustes coordinate data. Differences in each sections' shape were compared with a

◀ **Fig. 2** Quantitative polymerase chain reaction (qPCR) and Western blotting confirm ablation of Panx1 and Panx3. Skin (**a**), hindlimb (**b**), and cochleae (**c**), mRNA transcript levels for Panx1 and Panx3 were assessed using 18S rRNA or GAPDH to calculate normalized mRNA expression using the delta CT method. No Panx mRNA was found in the dKO tissues. Panx1 and Panx3 Western blots for P4 skin (**a**) and hindlimbs (**b**). Panx1 is glycosylated and runs in a multiple-banded pattern (Gly2, Gly1, Gly0) as shown in human embryonic kidney cells (HEK 293T) ectopically expressing Panx1 (bracket) and WT skin (not detectable in hindlimb). Panx3 protein (~ 43 kDa) shown in WT skin, bone, and transfected HEK 293T cells (bracket). Unspecific bands are evident at ~ 50 and 70 kDa (also in dKO). GAPDH was used as a loading control. Markers in kDa. Lines in blots indicate that positive control lanes (HEK Panx) are from the same blot but scanned at a lower intensity due to high ectopic expression. Bars, mean ± SEM. $N = 3$ in skin and limbs and $N = 4$ in cochleae. N, number of biological replicates

non-parametric MANOVA using the ProcD function in the R package *geomorph* ([37], R Foundation for Statistical Computing, Vienna, Austria, 2017); [38].

Principal component analyses

Differences in skull shape were compared using principal components analysis (PCA) performed on the variance/covariance matrix of Procrustes coordinates using the *geomorph* package in R [37]; R Foundation for Statistical Computing, Vienna, Austria, 2017). Scores for each individual for PC1 and PC2 are presented as a scatterplot. Differences in overall skull size as well as size of the cranial base, cranial vault, face, and mandible were compared using centroid size. Differences in size were compared using ANOVA and Tukey's post-hoc test. (details in Suppl. Methods).

Limb bone length comparisons

Limb bones of P0 dKO and WT mice were double-stained with alizarin red/alcian blue as previously described [39]. Differences in length for specific bones were determined using Welch's *t* tests with Bonferroni correction. All analyses were performed in R (R Foundation for Statistical Computing, Vienna, Austria, 2017). (details in Suppl. Methods).

Growth plate comparisons of P0 WT and dKO tibiae

Tibiae were dissected from a sample of six WT and five dKO P0 mice, fixed in 4% paraformaldehyde, decalcified, embedded in paraffin, and sectioned length-wise. Safranin-O/Fast Green staining was used to visualize the growth plate. Length of the proximal growth plate as well as the length of the proliferative and hypertrophic zones were measured using ImageJ and compared between WT and dKO mice using Welch's *t* tests in R.

Cross-sectional geometrical properties of humerus and femur

Cross-sectional measures were obtained from 20-μm thick cross-sections of the right humerus and femur from μCT scan data (see Suppl. Met.). Statistical comparison of each geometrical property was performed using Welch's two-sample *t* tests in R (R Foundation for Statistical Computing, Vienna, Austria, 2017) with Bonferroni corrections for multiple comparisons.

Hearing assessment using the auditory brainstem response (ABR)

Hearing levels were determined using the ABR technique, which was previously described [26]. For ABR waveform analysis, BioSig software program was used to measure the amplitudes and latencies of 90-dB sound pressure level (SPL) click stimuli for each wave and each mouse group tested. (details in Suppl. Methods).

Noise exposure

For a separate cohort of mice at 1 month of age, an initial ABR was followed immediately by exposure to a loud 12-kHz tonal stimulus at 115-dB SPL to both ears for a 1-h time period, as has been previously described [26].

Results

Characterization of dKO mice

Genotyping of dKO mice showed loss of both *Panx1* and *Panx3* (Fig. 1a). Although gross morphology of Panx1$^{-/-}$Panx3$^{-/-}$ mice (dKO) did not show any major differences, adult dKO mice were slightly smaller than WT as evidenced in representative pictures (Fig. 1b). Weaned litter sizes of dKO mice were significantly smaller compared to both WT and Panx1$^{-/-}$ weanlings (Fig. 1c). Additionally, overall body weight of dKO mice was significantly decreased at postnatal day 0 (P0), 2–3 months, and 16 months of age compared to aged-matched WT controls (Fig. 1d–f). However, qMRI tests revealed that the lean mass and fat mass normalized to body weight did not significantly change between WT and dKO mice at 2 months of age (Suppl. Fig. 1).

Panx1 and Panx3 are ablated in the skin, limb, and cochleae of dKO mice

Panx1 and Panx3 mRNA transcripts were present in the skin, hindlimb, and cochleae of WT mice and absent in dKO

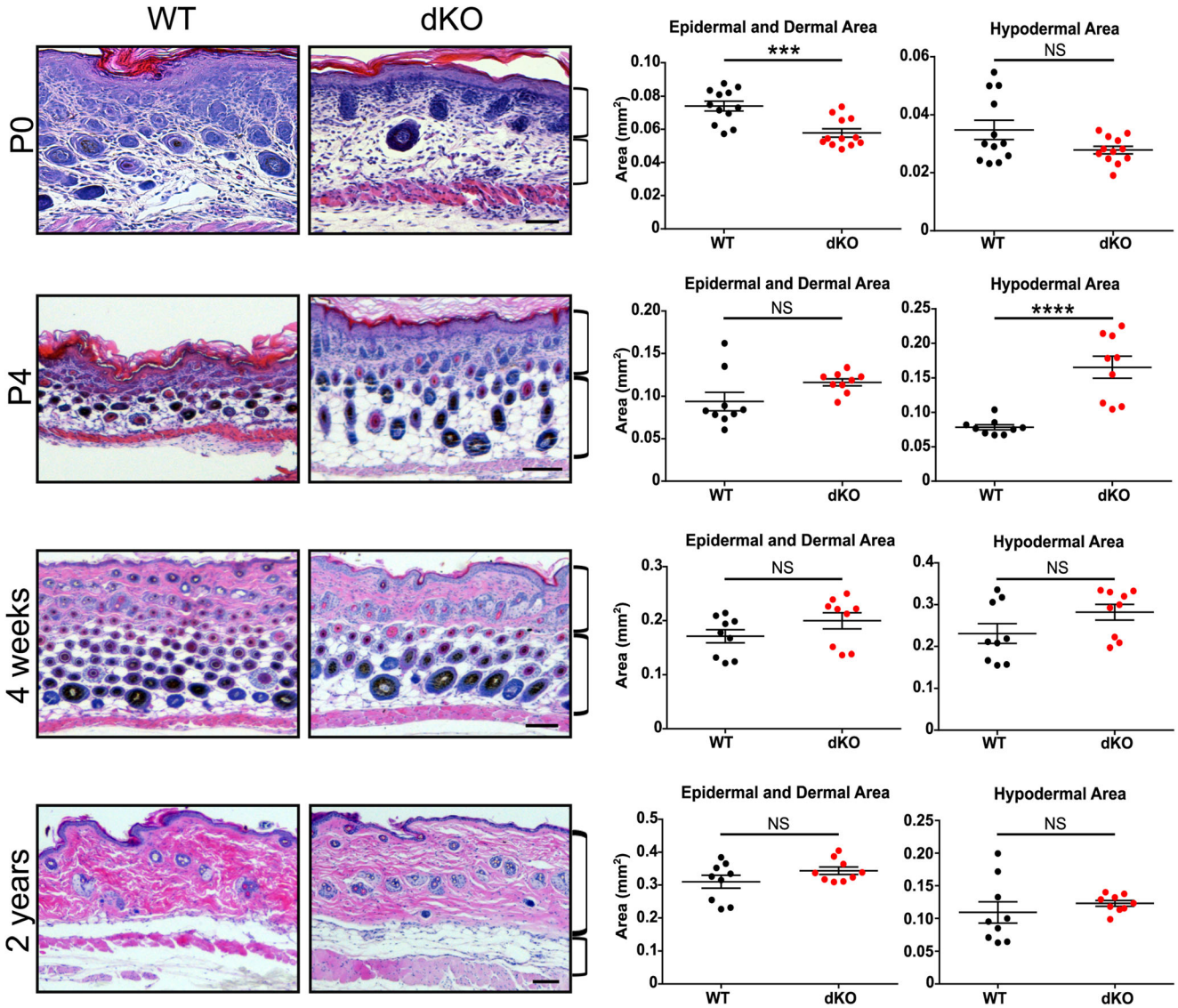

Fig. 3 In dKO mice dorsal skin, epidermal and dermal area is decreased at P0, and hypodermal area is increased at P4 compared to WT mice. Histological analysis of mouse dorsal skin at various ages showed the area of epidermal (excluding the highly variable stratum corneum) and dermal areas at P0, P4, 4 weeks, and 2 years of age in dKO and WT mice. $N = 3$, $n = 9$ for all time points and genotypes, except P0 ($N = 4$, $n = 12$). Error bars represent SEM. Scale bars represent 50 μm at P0 and 100 μm at P4, 4 weeks, and 2 years. N, biological replicates, n, technical replicates. Independent student t tests were performed. NS, no significance. ***$p < 0.001$, and ****$p < 0.0001$

(Fig. 2a–c). At the protein level, low but detectable amounts of Panx1 and Panx3 were observed in skin tissues which were ablated in dKO mice (Fig. 2a–c). In the hindlimb, Panx1 protein was undetectable in both WT and dKO, but high Panx3 protein expression was observed in WT mice (Fig. 2a–c). Other immunoreactive bands are apparent at 50 and 70 kD, but are not ablated in the dKO, indicating that they are unspecific. We assessed the expression of Panx2 and other large pore channels in WT and dKO tissues. In the skin, Panx2 full length was not detected, while Panx2 isoform X1 was observed at similar levels in WT and dKO mice (Suppl. Fig. 2A). Cx26, Cx30, and Cx43 mRNA transcripts were also similarly detected in both WT and dKO mice (Supplemental Fig. 2B). No differences in the expression of any of the tested Cxs or Panx2 channels were observed in WT and dKO hindlimbs or cochlear tissues (Supplemental Fig. 3A, B).

Fig. 4 Thick skin epidermal area is reduced in dKO paws of P0 mice. ▶ Histological analysis and area of measurements in the epidermal area of mouse thick paw skin at P0, P5, 4, 9, and 22 weeks of age was quantified. $N = 3$, $n = 9$, error bars represent SEM. Scale bars represent 25 μm. Unpaired student t tests were performed. NS, no significance; N, biological replicates; n, technical replicates. **$p < 0.01$

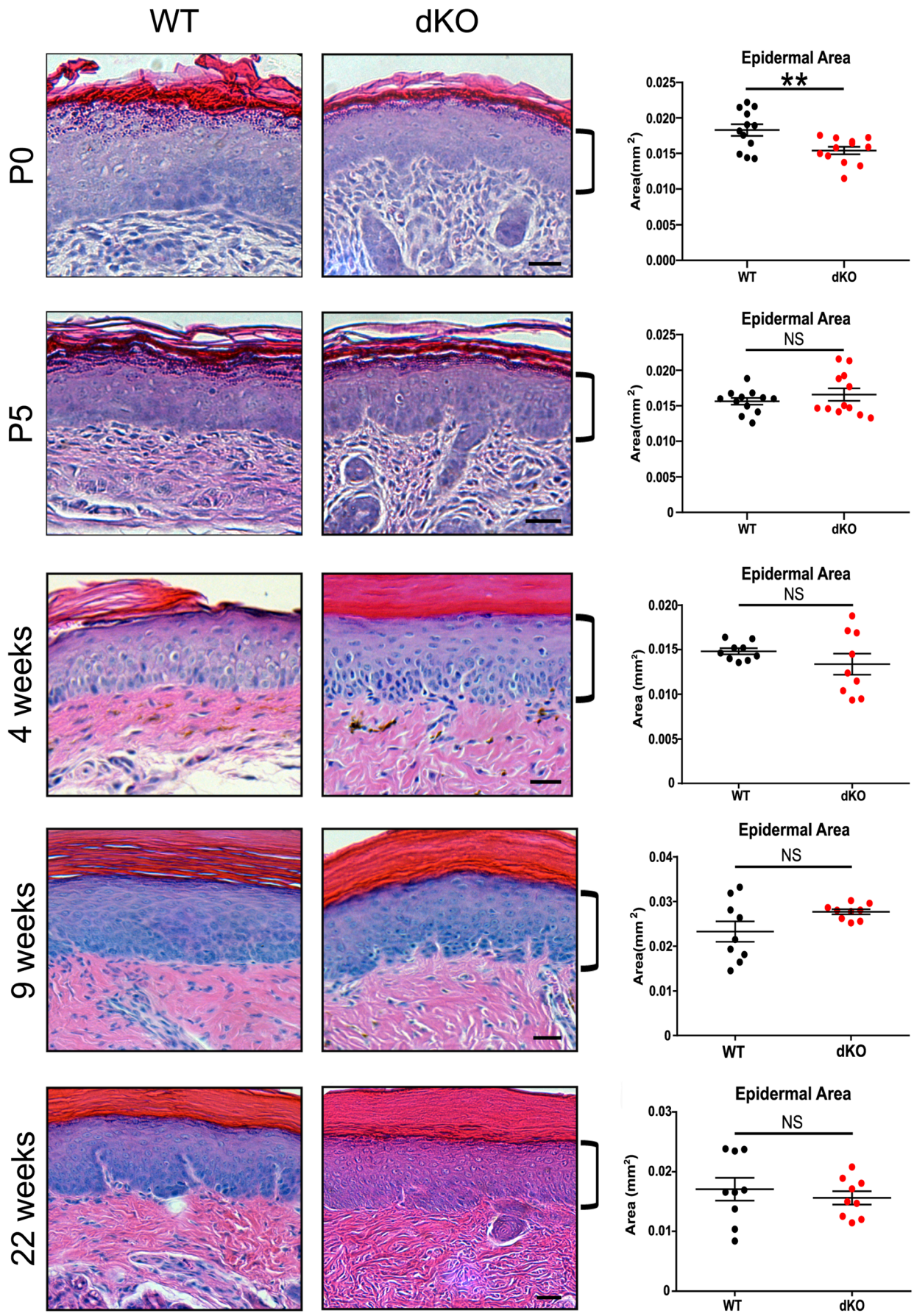
WT
dKO
P0
P5
4 weeks
9 weeks
22 weeks
Epidermal Area
**
NS
Area(mm 2)
Area (mm2)
0.025
0.020
0.015
0.010
0.005
0.000
0
0.04
0.03
0.02
0.01
WT
dKO

Neonatal dKO mice exhibit decreased epidermal and dermal area in dorsal and paw skin

Analysis of dorsal skin showed a significant decrease in the epidermal and dermal area of dKO mice at P0 compared to WT (Fig. 3). At P4, there was a significant increase in the hypodermal area of dKO compared to WT mice (Fig. 3). However, no significant differences were seen at any other time point (Fig. 3). dKO paw skin at P0 showed a significant decrease in epidermal area; however, no differences were found at any other age (Fig. 4a–c).

Skull shape is significantly altered in neonatal but not in adult dKO mice

Overall skull shape comparisons between dKO and WT mice at P0 was assessed using a MANOVA and found to be significant ($p = 0.00165$). Significant shape changes between dKO and WT mice were detected for all regions of the skull: face ($p = 0.00335$), base ($p = 0.00035$), cranial vault ($p = 0.00405$), and the mandible ($p = 0.00045$) at P0. However, at 3 months, no statistically significant shape changes were observed. Skull shape differences were visualized using principal component analyses (PCA). At P0, distinct separation was evident between WT and dKO mice across PC1 for the whole skull (Fig. 5a) as well as for each region of the skull, particularly in the cranial base (Fig. 5b). In contrast, in adult mice, there was no separation between genotypes across PC1 and PC2 (Fig. 5d, e). Heat morphs allow visualization of shape changes in P0 dKO across PC1 (Fig. 5c, f).

dKO mice have significantly smaller mandibles, shorter hind limbs, and altered femoral and humeral cross-sectional properties

Size of the whole skull, face, cranial base, and cranial vault did not differ significantly between genotypes at P0 or in adult mice (Fig. 5g). Mandible size was significantly smaller in dKO mice at P0 and at 3 months (Fig. 5g). Lengths of the ossified portion of fore- and hind limb bones of P0 pups were measured and showed that P0 dKO mice have significantly shorter hind limb bones than WT (Fig. 6a). Qualitative assessment revealed no differences in the general histomorphology of the tibial growth plate between WT and dKO P0 mice (Fig. 6c). Measures of growth plate length were not statistically different between genotypes. Similarly, proportional lengths of the prehypertrophic and hypertrophic zones relative to total growth plate length were similar between genotypes (Fig. 6d). At P0, polar second moment of area (J) ($p = 0.0000034$) and cortical area (CA) ($p = 0.0024$) of the humerus are larger in dKO than WT mice (Fig. 6e). At 3 months, dKO mice have significantly larger %CA of the humerus than WT mice ($p = 0.014$) and significantly larger femur Imax/Imin ($p = 0.009$) (Fig. 6e).

Fig. 5 Skull shape is altered in dKO mice compared to WT mice at P0 but not in adult mice. Principal components analyses (PCA) were used to visualize differences in shape between dKO and WT mice at P0 for the whole skull, face, cranial base, cranial vault, and mandible. Small circles represent PC scores for PC1 and PC2 for each individual; large circles represent the average score for each genotype along PC1 and PC2. The two genotypes are clearly separated along PC1 for all regions of the skull at P0 (**a**, **b**). At 3 months (adult), no clear separation between genotypes was found for any of the regions analyzed (**d**, **e**). Specific shape changes associated with variation across PC1 are represented as heat morphs (**c**, **f**). Red coloration demonstrates regions of the skull that differ the most between the average dKO mouse and the group mean, whereas gray coloration represents differences between the average WT mouse and the group mean. At P0, the greatest shape differences in dKO mice are found in the cranial vault and cranial base (**c**), in agreement with our regional PC plots (**b**). At 3 months, the main differences in skull shape are concentrated on the inferior surface of the cranial base and face (**f**). Note that while these regions of the skull look markedly different due to the red color, the actual difference (< 0.5 mm) is quite small for an adult mouse skull. Overall skull size, as well as face, cranial base, cranial vault, and mandibular size were compared between dKO and WT mice at P0 and 3 months. For both age groups, WT mice have significantly larger mandibles than dKO mice (**g**). $^{**}p < 0.01$

dKO mice have normal hearing

Representative ABR trace recordings of WT and dKO mice for a click stimulus showed that ABRs were similar in both genotypes (Fig. 7a). No significant differences were observed between WT and dKO mice at any of the stimuli tested (Fig. 7b). In addition to measuring hearing thresholds, analysis of ABR waveforms provided an indication of the integrity of neurotransmission throughout the auditory brainstem. dKO mice had significantly larger amplitudes in wave I (cochlear nerve), wave III (superior olivary complex), and wave IV (lateral lemniscus/inferior colliculus) of the ABR, findings which could result from a greater number of neurons along the auditory pathway being activated by the acoustic stimulus, and/or because the population of neurons in a given brainstem region discharged with more precise timing following each of the 1000 acoustic stimulus presentations (i.e., less variability in the timing of the discharges across presentations; increased neural synchrony) compared to WTs (Fig. 7c). That said, no differences were detected in the latencies of ABR waveforms in dKO (Fig. 7d), suggesting that the speed of neurotransmission was not affected by genotype. Collectively, these data suggest that dKO mice do not exhibit hearing deficits, and even have enhanced activation and/or neural synchrony in distinct auditory brainstem regions.

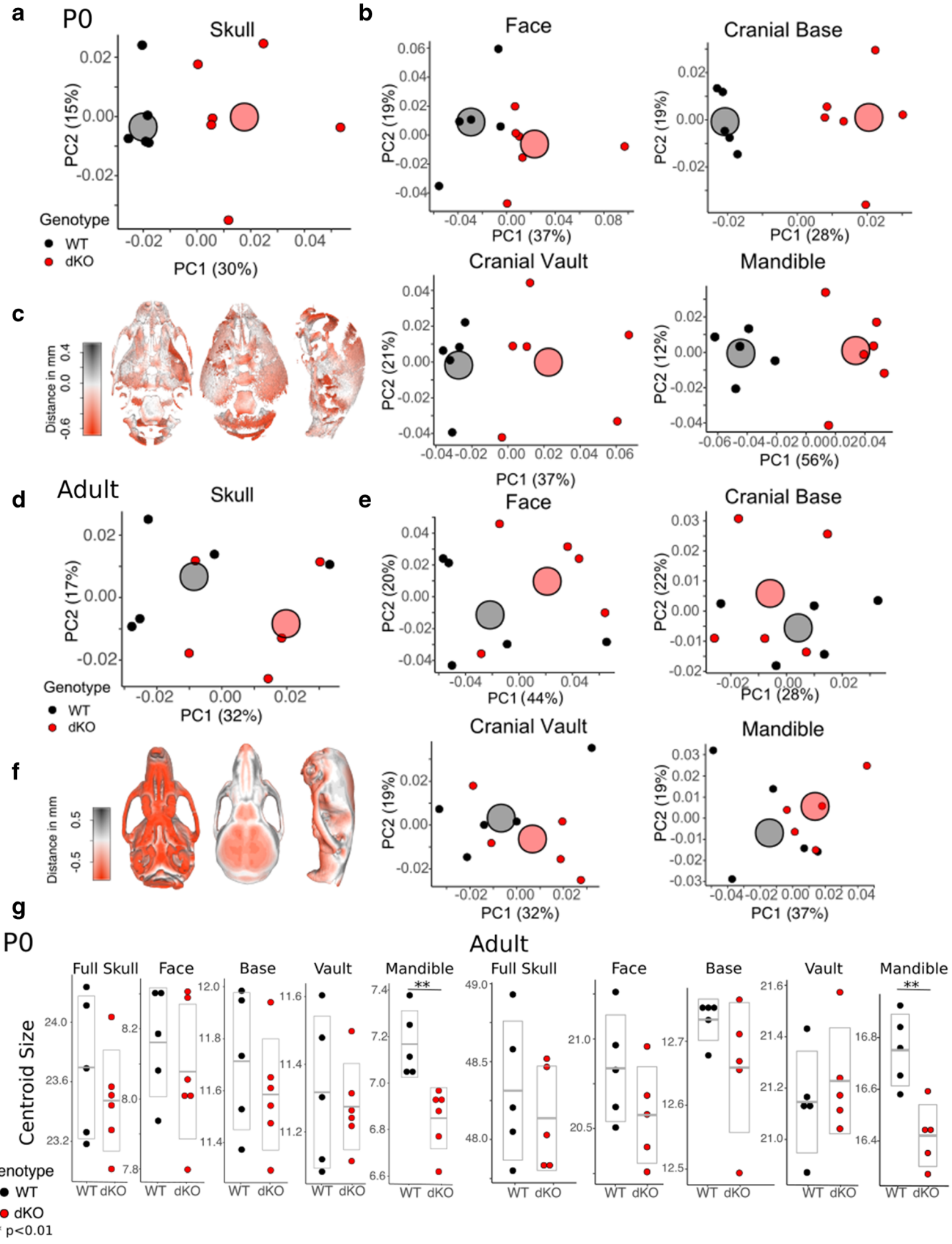
a
P0
Skull
PC2 (15%)
PC1 (30%)
Genotype
WT
dKO
b
Face
PC2 (19%)
PC1 (37%)
Cranial Base
PC2 (19%)
PC1 (28%)
Cranial Vault
PC2 (21%)
PC1 (37%)
Mandible
PC2 (12%)
PC1 (56%)
c
Distance in mm
d
Adult
Skull
PC2 (17%)
PC1 (32%)
Genotype
WT
dKO
e
Face
PC2 (20%)
PC1 (44%)
Cranial Base
PC2 (22%)
PC1 (28%)
Cranial Vault
PC2 (19%)
PC1 (32%)
Mandible
PC2 (19%)
PC1 (37%)
f
Distance in mm
g
P0
Adult
Full Skull
Face
Base
Vault
Mandible
Centroid Size
Genotype
WT
dKO
** p<0.01

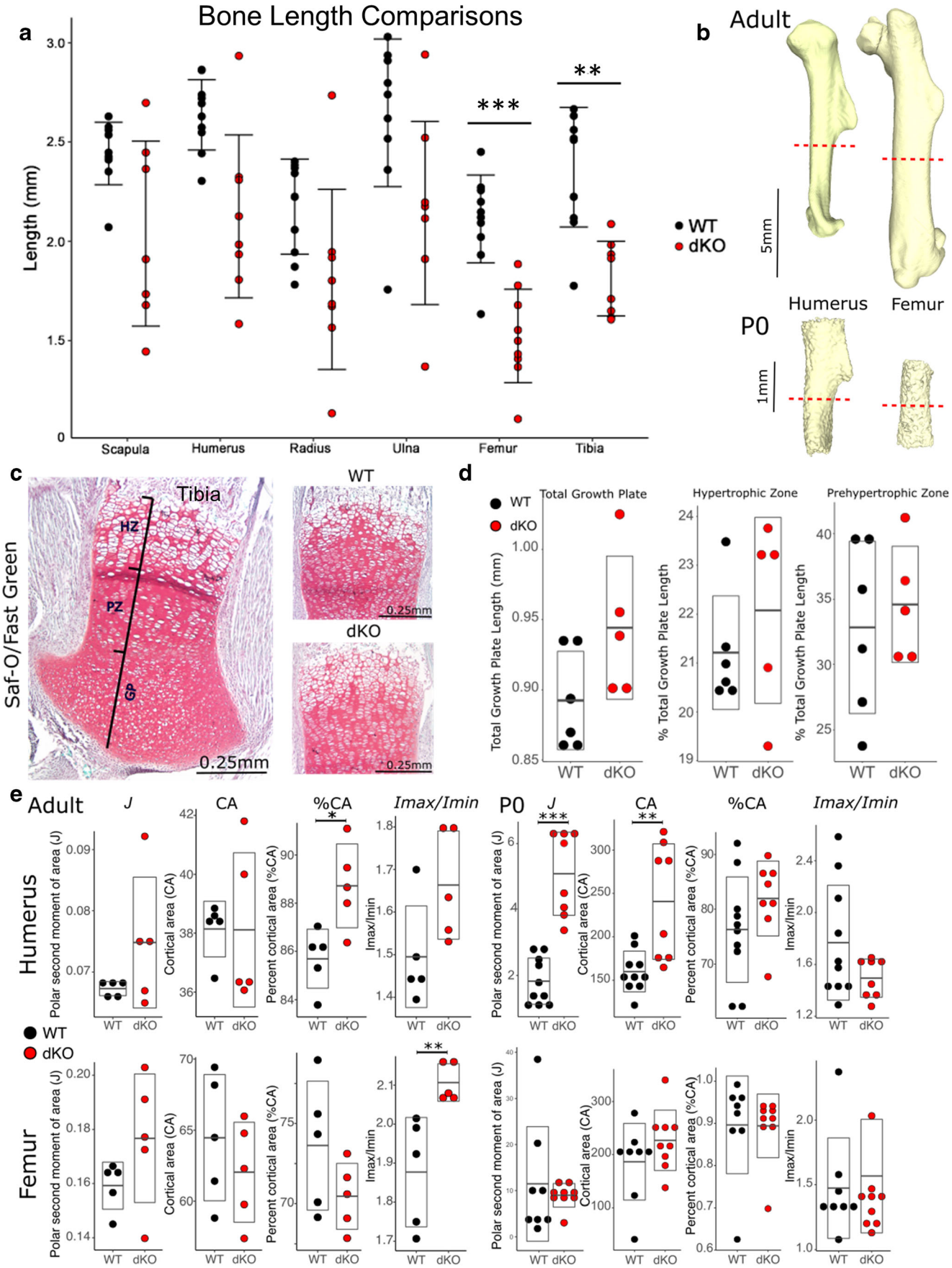
a
Bone Length Comparisons
Length (mm)
3.0
2.5
2.0
1.5
0
Scapula
Humerus
Radius
Ulna
Femur
Tibia
***
**
b
Adult
WT
dKO
5mm
Humerus
Femur
P0
1mm
c
Saf-O/Fast Green
Tibia
HZ
PZ
GP
0.25mm
WT
dKO
0.25mm
0.25mm
d
WT
dKO
Total Growth Plate
Total Growth Plate Length (mm)
1.00
0.95
0.90
0.85
WT
dKO
Hypertrophic Zone
% Total Growth Plate Length
24
23
22
21
20
19
WT
dKO
Prehypertrophic Zone
% Total Growth Plate Length
40
35
30
25
WT
dKO
e
Adult
J
CA
%CA
Imax/Imin
P0
J
CA
%CA
Imax/Imin
Humerus
Femur
Polar second moment of area (J)
Cortical area (CA)
Percent cortical area (%CA)
Imax/Imin
WT
dKO
*
***
**
**

◀ **Fig. 6** dKO mice have significantly shorter hind limb bones than WT mice and altered femoral and humeral cross-sectional properties. At P0, measures of femoral and tibial lengths are significantly shorter in dKO compared with WT mice (**a**). Geometric properties of the humerus and femur were calculated from diaphyseal cross-sections as shown (**b**). The general organization of the proximal tibial growth plate (GP), proliferative zone (PZ), and hypertrophic zone (HZ) is similar between genotypes at P0 (**c**), and no differences were found between dKO and WT mice for length measures of the total growth plate, or the prehypertrophic or hypertrophic zones as measured as percent of the total growth plate (**d**). Analysis of (**b**), showed that humeri of dKO mice have significantly larger cortical area (CA) and polar second moment of area (J) than WT mice at P0, while at 3 months, percent cortical area (%CA) is significantly larger in dKO mice (**e**). No significant differences in femur cross-sectional measurements were detected at P0 between genotypes, but at 3 months, dKO mice have significantly larger Imax/Imin values (**e**).*$p < 0.05$, **$p < 0.001$, ***$p < 0001$

dKO mice have slightly decreased susceptibility to noise-induced hearing loss

As expected, ABR thresholds to all stimuli (click, 4–24-kHz tones) were elevated immediately after the noise exposure in both WT and dKO mice (Fig. 8a–d), with the greatest degree of hearing impairment evident at the higher frequencies (Fig. 8c–d). Interestingly, 7 days after the noise exposure, the 24-kHz hearing thresholds of dKO mice had recovered to a greater degree (i.e., lower ABR threshold values) than the WT mice, findings which show that the dKO mice were slightly less susceptible to permanent noise-induced hearing loss (Fig. 8d).

Discussion

Single pannexin knockout mice have been used to assess the impacts of Panx channels in various organs [3]. However, recent findings suggest potential compensatory mechanisms between Panx family members, reinforcing that double knock-out (dKO) mice are necessary to examine their true functions within different organ systems. We created the first Panx1 and Panx3 dKO mouse model which was not trivial, since both *Panx1* and *Panx3* genes are closely located in chromosome 9 within 22 Mb of each other in the mouse genome (NCBI), thus making the recombination efficiency of this event very low.

dKO mice showed decreased body weight, and this change was not previously observed in either of the two single KO models of Panx1 and Panx3 [24, 32]. However, qMRI of adult dKO mice did not show any differences in fat mass or lean mass, when normalized to body weight (Supplemental Fig. 1 A, B). In addition, dKO mice had significantly decreased litter sizes (fewer pups per litter) compared to controls, a finding

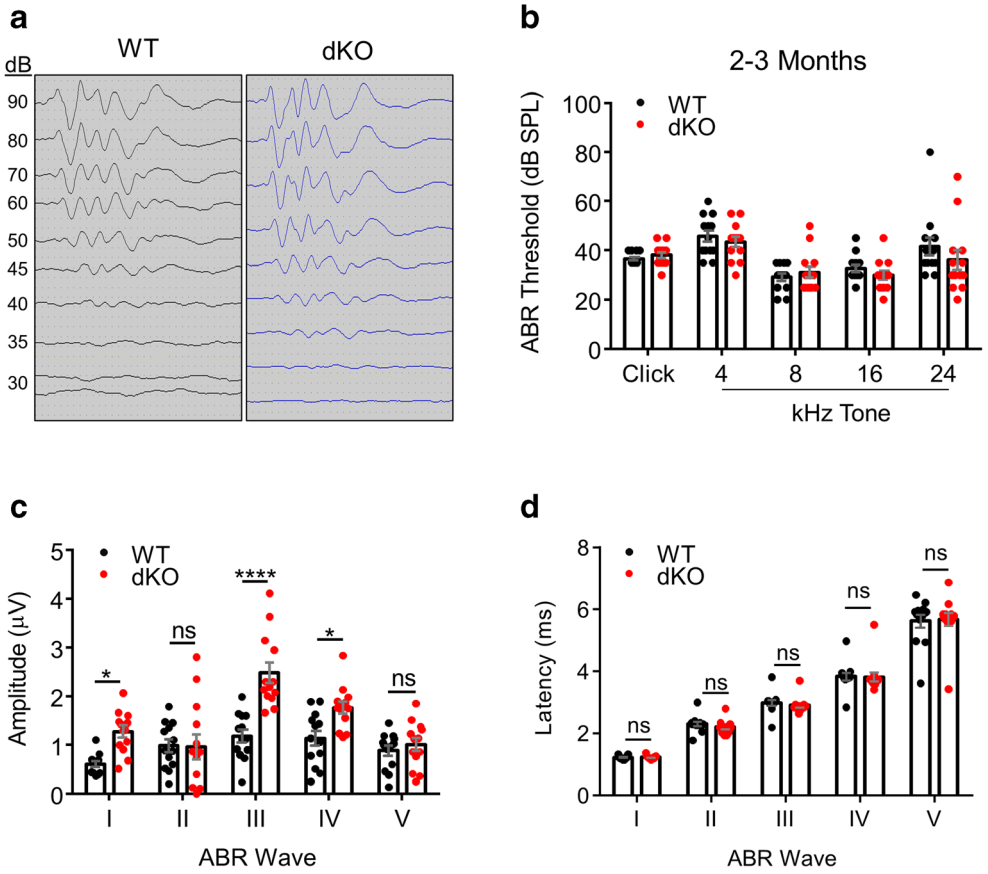

Fig. 7 Double knockout mice have normal hearing. Representative auditory brainstem response (ABR) traces of a broadband click stimulus in both WT and dKO mice (**a**). Hearing assessment of 2–3-month-old mice through ABRs of WT and dKO mice for a broadband click stimulus and tonal specific frequencies (4, 8, 16, and 24 kHz tones) (**b**). ABR waveforms were further analyzed at the 90-dB click stimulus by their amplitudes (**c**) and latencies (**d**), representing neural synchrony and speed, respectively. Bars represent mean ± SEM. *$p < 0.05$, ****$p < 0.0001$, one-way ANOVA followed by Sidak's post-hoc tests. Ns, no significance. WT, $N = 12$; dKO, $N = 13$. One outlier, as determined by GraphPad was removed from (**b**). N, number of biological replicates

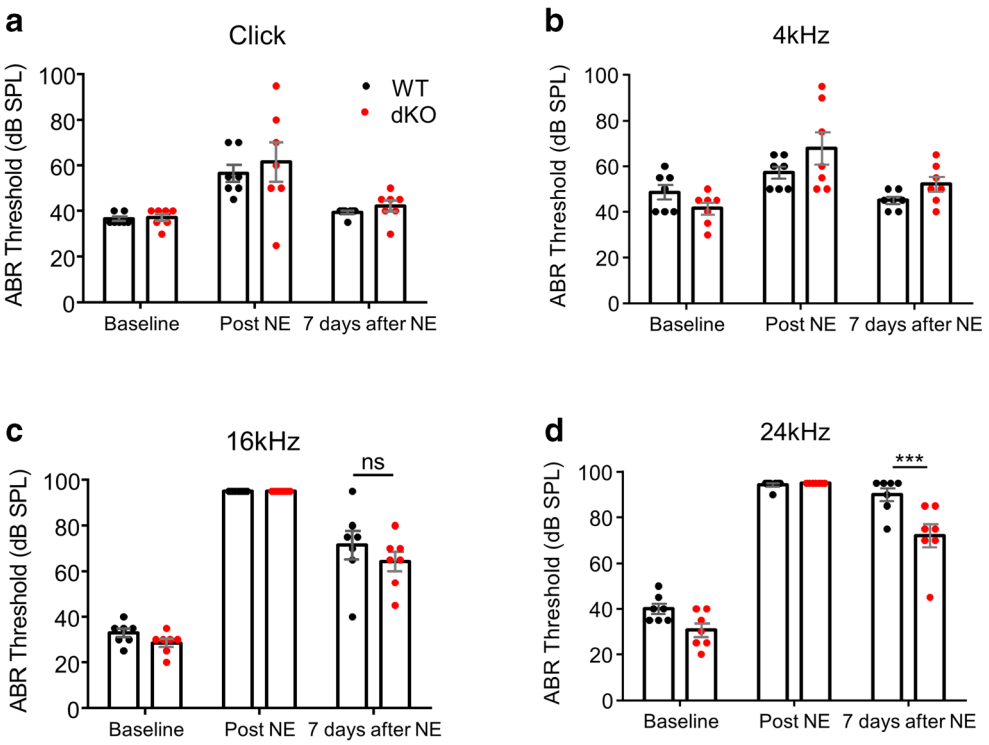

Fig. 8 dKO mice exhibit slight protection against noise-induced hearing loss. Noise exposure (NE) increased ABR thresholds immediately after NE (post NE) for all stimuli tested, confirming auditory damage in both WT and dKO mice (**a**–**d**). The highest ABR thresholds were found at the higher frequency stimuli 16 kHz (**c**) and 24 kHz (**d**) tones. $N = 7$ for each genotype. Bars represent mean ± SEM. Two-way repeated measures ANOVA with Sidak's post-hoc tests were performed for each individual stimulus. ***$p < 0.001$, N number of biological replicates

that was also shown for Panx3$^{-/-}$ mice [24] and that may be due to higher intra-uterine death but remains to be studied.

At P0, dKO mice had reduced dorsal skin thickness which was similarly found in our previous study for Panx1$^{-/-}$ mice [17]. At P4, however, this finding was no longer evident and instead dKO mice exhibited increased hypodermal area where subcutaneous fat is found. The Panx1$^{-/-}$ mice also had a significant increase in hypodermal area and an increase in overall fat content due to the enhanced differentiation capacity of adipose stromal cells from the Panx1$^{-/-}$ to form adipocytes with higher fat content [40].

While an overt skeletal phenotype has not been associated with Panx1 KO mice, Panx3 KO mice have been reported to have shortened long bones and hypomineralization of the skull and long bones [25, 41, 42]. Thus, the relatively mild skeletal phenotype observed in our dKO mice is unexpected, but similar to our previous report on the bone morphology of the global Panx3 KO mouse [25].

While we found significant skull shape differences between dKO and WT mice at P0, by 3 months, dKO mouse skull morphology appeared to "recover." This could be due to a combination of the minor phenotypic effects observed at P0 coupled with the rapid growth and remodeling of the mouse skull within the first 2 months of postnatal development [25]. The main skull shape changes we observed in dKO mice at P0 were localized to the cranial base and cranial vault. Early postnatal growth of these regions is quite rapid, plateauing by P14-P21 in mice [43].

Tibial and femoral lengths were shorter in dKO than WT mice at P0. However, no differences in tibial growth plates were observed at P0 between genotypes suggesting that subsequent tibial growth would be similar to WT, potentially enabling recovery of the phenotype through postnatal development. For the humerus, cortical area (CA) and polar second moment of area (J) are significantly larger in dKO mice than WT at P0, suggesting that dKO humeri have an increased resistance to compressive and torsional forces respectively. By 3 months, CA and J of the humerus are similar between genotypes but the proportion of cortical area to total subperiosteal area (%CA) is significantly greater in dKO mice, indicating thicker cortical bone. At 3 months, dKO mice have significantly larger Imax/Imin ratios for the femur which indicates that the distribution of cortical bone within the cross-section is altered. Previously, we reported that humeri and femora of adult Panx3 KO mice have increased J and CA compared to WT mice [25]. While we expected similar results in our dKO model, it appears that knocking out both genes results in a phenotype separate from the single Panx3 KO.

Previous studies showed that a conditional ablation of Panx1 in the cochlea resulted in severe hearing loss [27]. Additionally, a human patient harboring a Panx1 mutation was found to exhibit many clinical symptoms including hearing loss [44]. In contrast, another Panx1$^{-/-}$ mouse had normal hearing and did not exhibit any auditory brainstem morphology deformities [26]. Recently, that same Panx1$^{-/-}$ model was found to have mild hearing loss at low frequencies which was more pronounced at higher frequencies (i.e., 32 and 40 kHz) [45]. Zorzi and colleagues re-examined

the auditory phenotype of the first-generated Panx1$^{-/-}$ mice and found that they did not have hearing loss [46]. To rule out the possibility that in the global Panx1 KO, Panx3 could be compensating for its function, we tested the dKO hearing and found that both pannexins are dispensable for hearing function. In fact, dKO mice had increased ABR wave amplitudes representing enhancement of the neural synchrony within these auditory brainstem regions.

The double deletion of Panx1/Panx3 did not show more overt phenotypes than the single KO models and in some cases, reduced the severity of the phenotypes observed. As with Panx1 and Panx3 single KOs, we might see more pronounced phenotypes once they are challenged with different insults. In the dKO, there was no upregulation of Panx2 and connexins known to be expressed in some of these tissues [11, 47–49], plus in hindlimb, we could not detect any expression of Panx2, Cx26, or Cx30 (Suppl. Fig. 3A). However, it is possible that these and other large pore channels can still functionally compensate for the missing Panxs deleted from germline throughout development. Therefore, in some instances, the use of conditional KOs may be necessary to avoid this potential issue with compensation that could mask some phenotypes. In conclusion, we have shown that dKO mice have alterations in the skin and bone at early stages but do not exhibit hearing loss and show better recovery upon noise damage. Our findings sugggest that Panx1 and Panx3 may be important in early development of musculoskeletal tissues but are not required for hearing.

Acknowledgements We thank Genentech Inc. (San Francisco, CA) for the gift of the Panx1 knockout mouse, Rafael Sanchez Pupo for technical assistance, and Quintyn Farrar for his help collecting long bone data. JMA was funded by a Natural Sciences and Engineering Research Council (NSERC) Scholarship. BO and CBW were funded by an Ontario Graduate Scholarship (OGS). EJ and CBW received the Collaborative Specialization in Musculoskeletal Health Research (CMHR) award. NSERC Discovery Grant to KW. CIHR Project grant to BLA. NSERC Discovery Grant to SP.

Author contributions JMA: Mouse genotyping, conducted all hearing experiments, data collection, and analysis, compilation of all experimental data, and wrote the manuscript draft.

BO'D: Mouse genotyping, expression analyses of skin and hindlimb, histological analyses of skin and paw.

CBW: Mouse genotyping, qPCR and protein experiments, data collection, and analysis.

EJ: Skull data collection and analysis, histological analysis of tibial growth plate and long bone cross-sectional analyses.

JJK: Conceptualization of the dKO hearing study, student training, data analysis.

KB: Generated the dKO mice, performed initial characterization and limb bone length comparisons, and contributed to skull landmarking.

KW: Skull and limb phenotypic analyses, provided funding.

BLA: Analyses and interpretation of hearing testing, provided funding.

SP: Generation of the dKO mice, initial characterization experiments, study design, provided funding, supervised and coordinated all participants, data analysis, manuscript editing.

All authors participated in manuscript editing.

Compliance with ethical standards

Conflict of interest The authors declare that they have no competing interests.

References

1. Panchin Y, Kelmanson I, Matz M, Lukyanov K, Usman N, Lukyanov S (2000) A ubiquitous family of putative gap junction molecules. Curr Biol 10:R473–R474
2. Baranova A, Ivanov D, Petrash N, Pestova A, Skoblov M, Kelmanson I, Shagin D, Nazarenko S, Geraymovych E, Litvin O, Tiunova A, Born TL, Usman N, Staroverov D, Lukyanov S, Panchin Y (2004) The mammalian pannexin family is homologous to the invertebrate innexin gap junction proteins. Genomics 83:706–716
3. Penuela S, Gehi R, Laird DW (2013) The biochemistry and function of pannexin channels. Biochim Biophys Acta 1828:15–22
4. Sosinsky GE, Boassa D, Dermietzel R, Duffy HS, Laird DW, MacVicar B, Naus CC, Penuela S, Scemes E, Spray DC, Thompson RJ, Zhao HB, Dahl G (2011) Pannexin channels are not gap junction hemichannels. Channels (Austin) 5:193–197
5. Scemes E, Spray DC, Meda P (2009) Connexins, pannexins, innexins: novel roles of "hemi-channels". Pflugers Arch 457:1207–1226
6. Bruzzone R, Hormuzdi SG, Barbe MT, Herb A, Monyer H (2003) Pannexins, a family of gap junction proteins expressed in brain. Proc Natl Acad Sci U S A 100:13644–13649
7. Penuela S, Bhalla R, Nag K, Laird DW (2009) Glycosylation regulates pannexin intermixing and cellular localization. Mol Biol Cell 20:4313–4323
8. Ray A, Zoidl G, Weickert S, Wahle P, Dermietzel R (2005) Site-specific and developmental expression of pannexin1 in the mouse nervous system. Eur J Neurosci 21:3277–3290
9. Wang XH, Streeter M, Liu YP, Zhao HB (2009) Identification and characterization of pannexin expression in the mammalian cochlea. J Comp Neurol 512:336–346
10. Tang W, Ahmad S, Shestopalov VI, Lin X (2008) Pannexins are new molecular candidates for assembling gap junctions in the cochlea. Neuroreport 19:1253–1257
11. Le Vasseur M, Lelowski J, Bechberger JF, Sin WC, Naus CC (2014) Pannexin 2 protein expression is not restricted to the CNS. Front Cell Neurosci 8:392
12. Turmel P, Dufresne J, Hermo L, Smith CE, Penuela S, Laird DW, Cyr DG (2011) Characterization of pannexin1 and pannexin3 and their regulation by androgens in the male reproductive tract of the adult rat. Mol Reprod Dev 78:124–138
13. Bao L, Locovei S, Dahl G (2004) Pannexin membrane channels are mechanosensitive conduits for ATP. FEBS Lett 572:65–68
14. Locovei S, Wang J, Dahl G (2006) Activation of pannexin 1 channels by ATP through P2Y receptors and by cytoplasmic calcium. FEBS Lett 580:239–244
15. Chekeni FB, Elliott MR, Sandilos JK, Walk SF, Kinchen JM, Lazarowski ER, Armstrong AJ, Penuela S, Laird DW, Salvesen GS, Isakson BE, Bayliss DA, Ravichandran KS (2010) Pannexin 1 channels mediate 'find-me' signal release and membrane permeability during apoptosis. Nature 467:863–867
16. Penuela S, Bhalla R, Gong XQ, Cowan KN, Celetti SJ, Cowan BJ, Bai D, Shao Q, Laird DW (2007) Pannexin 1 and pannexin 3 are glycoproteins that exhibit many distinct characteristics from the connexin family of gap junction proteins. J Cell Sci 120:3772–3783

17. Penuela S, Kelly JJ, Churko JM, Barr KJ, Berger AC, Laird DW (2014) Panx1 regulates cellular properties of keratinocytes and dermal fibroblasts in skin development and wound healing. J Invest Dermatol 134:2026–2035
18. Celetti SJ, Cowan KN, Penuela S, Shao Q, Churko J, Laird DW (2010) Implications of pannexin 1 and pannexin 3 for keratinocyte differentiation. J Cell Sci 123:1363–1372
19. Cowan KN, Langlois S, Penuela S, Cowan BJ, Laird DW (2012) Pannexin1 and Pannexin3 exhibit distinct localization patterns in human skin appendages and are regulated during keratinocyte differentiation and carcinogenesis. Cell Commun Adhes 19:45–53
20. Zhang P, Ishikawa M, Rhodes C, Doyle A, Ikeuchi T, Nakamura K, Chiba Y, He B, Yamada Y (2018) Pannexin-3 deficiency delays skin wound healing in mice due to defects in channel functionality. J Invest Dermatol 139(4):909–918
21. Bond SR, Lau A, Penuela S, Sampaio AV, Underhill TM, Laird DW, Naus CC (2011) Pannexin 3 is a novel target for Runx2, expressed by osteoblasts and mature growth plate chondrocytes. J Bone Miner Res 26:2911–2922
22. Ishikawa M, Yamada Y (2017) The role of Pannexin 3 in bone biology. J Dent Res 96:372–379
23. Ishikawa M, Iwamoto T, Nakamura T, Doyle A, Fukumoto S, Yamada Y (2011) Pannexin 3 functions as an ER Ca(2+) channel, hemichannel, and gap junction to promote osteoblast differentiation. J Cell Biol 193:1257–1274
24. Moon PM, Penuela S, Barr K, Khan S, Pin CL, Welch I, Attur M, Abramson SB, Laird DW, Beier F (2015) Deletion of Panx3 prevents the development of surgically induced osteoarthritis. J Mol Med (Berl) 93:845–856
25. Caskenette D, Penuela S, Lee V, Barr K, Beier F, Laird DW, Willmore KE (2016) Global deletion of Panx3 produces multiple phenotypic effects in mouse humeri and femora. J Anat 228:746–756
26. Abitbol JM, Kelly JJ, Barr K, Schormans AL, Laird DW, Allman BL (2016) Differential effects of pannexins on noise-induced hearing loss. Biochem J 473:4665–4680
27. Chen J, Zhu Y, Liang C, Zhao HB (2015) Pannexin1 channels dominate ATP release in the cochlea ensuring endocochlear potential and auditory receptor potential generation and hearing. Sci Rep 5:10762
28. Zhao HB, Zhu Y, Liang C, Chen J (2015) Pannexin 1 deficiency can induce hearing loss. Biochem Biophys Res Commun 463:143–147
29. Bargiotas P, Krenz A, Hormuzdi SG, Ridder DA, Herb A, Barakat W, Penuela S, von Engelhardt J, Monyer H, Schwaninger M (2011) Pannexins in ischemia-induced neurodegeneration. Proc Natl Acad Sci U S A 108:20772–20777
30. Lohman AW, Billaud M, Straub AC, Johnstone SR, Best AK, Lee M, Barr K, Penuela S, Laird DW, Isakson BE (2012) Expression of pannexin isoforms in the systemic murine arterial network. J Vasc Res 49:405–416
31. Whyte-Fagundes P, Kurtenbach S, Zoidl C, Shestopalov VI, Carlen PL, Zoidl G (2018) A potential compensatory role of Panx3 in the VNO of a Panx1 Knock out mouse model. Front Mol Neurosci 11:135
32. Qu Y, Misaghi S, Newton K, Gilmour LL, Louie S, Cupp JE, Dubyak GR, Hackos D, Dixit VM (2011) Pannexin-1 is required for ATP release during apoptosis but not for inflammasome activation. J Immunol 186:6553–6561
33. Hill CA, Sussan TE, Reeves RH, Richtsmeier JT (2009) Complex contributions of Ets2 to craniofacial and thymus phenotypes of trisomic "Down syndrome" mice. Am J Med Genet A 149A:2158–2165
34. Motch Perrine SM, Cole TM 3rd, Martinez-Abadias N, Aldridge K, Jabs EW, Richtsmeier JT (2014) Craniofacial divergence by distinct prenatal growth patterns in Fgfr2 mutant mice. BMC Dev Biol 14:8
35. Martinez-Abadias N, Holmes G, Pankratz T, Wang Y, Zhou X, Jabs EW, Richtsmeier JT (2013) From shape to cells: mouse models reveal mechanisms altering palate development in Apert syndrome. Dis Model Mech 6:768–779
36. Adams DC, Otarola-Castillo E (2013) Geomorph: an r package for the collection and analysis of geometric morphometric shape data. Methods Ecol Evol 4:393–399
37. Adams DC, Collyer ML, Kaliontzopoulou A (2018) Geometric morphometric analyses of 2D/3D landmark data (Version 3.07)
38. Collyer ML, Sekora DJ, Adams DC (2015) A method for analysis of phenotypic change for phenotypes described by high-dimensional data. Heredity (Edinb) 115:357–365
39. McLeod MJ (1980) Differential staining of cartilage and bone in whole mouse fetuses by alcian blue and alizarin red S. Teratology 22:299–301
40. Lee V, Barr KJ, Kelly J, Johnston D, Brown C, Robb K, Sayedyahossein S, Huang K, Gros R, Flynn L et al (2018) Pannexin 1 regulates adipose stromal cell differentiation and fat accumulation. Sci Rep 8:16166
41. Oh SK, Shin JO, Baek JI, Lee J, Bae JW, Ankamerddy H, Kim MJ, Huh TL, Ryoo ZY, Kim UK, Bok J, Lee KY (2015) Pannexin 3 is required for normal progression of skeletal development in vertebrates. FASEB J 29:4473–4484
42. Ishikawa M, Williams GL, Ikeuchi T, Sakai K, Fukumoto S, Yamada Y (2016) Pannexin 3 and connexin 43 modulate skeletal development through their distinct functions and expression patterns. J Cell Sci 129:1018–1030
43. Vora SR, Camci ED, Cox TC (2015) Postnatal ontogeny of the cranial base and craniofacial skeleton in male C57BL/6J mice: a reference standard for quantitative analysis. Front Physiol 6:417
44. Shao Q, Lindstrom K, Shi R, Kelly J, Schroeder A, Juusola J, Levine KL, Esseltine JL, Penuela S, Jackson MF, Laird DW (2016) A germline variant in the PANX1 gene has reduced channel function and is associated with multisystem dysfunction. J Biol Chem 291:12432–12443
45. Chen J, Liang C, Zong L, Zhu Y, Zhao HB (2018) Knockout of Pannexin-1 induces hearing loss. Int J Mol Sci 19
46. Zorzi V, Paciello F, Ziraldo G, Peres C, Mazzarda F, Nardin C, Pasquini M, Chiani F, Raspa M, Scavizzi F, Carrer A, Crispino G, Ciubotaru CD, Monyer H, Fetoni AR, M. Salvatore A, Mammano F (2017) Mouse Panx1 is dispensable for hearing acquisition and auditory function. Front Mol Neurosci 10:379
47. Forge A, Becker D, Casalotti S, Edwards J, Marziano N, Nevill G (2003) Gap junctions in the inner ear: comparison of distribution patterns in different vertebrates and assessement of connexin composition in mammals. J Comp Neurol 467:207–231
48. Plotkin LI, Bellido T (2013) Beyond gap junctions: Connexin43 and bone cell signaling. Bone 52:157–166
49. Xu J, Nicholson BJ (2013) The role of connexins in ear and skin physiology - functional insights from disease-associated mutations. Biochim Biophys Acta 1828:167–178